

## Effects of loading a magnetic field longitudinal to the linear particle-beam track on yields of reactive oxygen species in water

Ken-ichiro Matsumoto<sup>a</sup>, Ikuo Nakanishi<sup>b</sup>, Yasushi Abe<sup>c</sup>, Shinji Sato<sup>c</sup>, Ryosuke Kohno<sup>c</sup>, Dousatsu Sakata<sup>c</sup>, Kota Mizushima<sup>c</sup>, Sung Hyun Lee<sup>c</sup> and Taku Inaniwa<sup>a</sup>

<sup>a</sup>Quantitative RedOx Sensing Group, Department of Radiation Regulatory Science Research, National Institute of Radiological Sciences, Quantum Life and Medical Science Directorate, National Institutes for Quantum and Radiological Science and Technology, Chiba-shi, Japan; <sup>b</sup>Quantum RedOx Chemistry Group, Institute for Quantum Life Science, Quantum Life and Medical Science Directorate, National Institutes for Quantum and Radiological Science and Technology, Chiba-shi, Japan; <sup>c</sup>Department of Accelerator and Medical Physics, Institute for Quantum Medical Science, Quantum Life and Medical Science Directorate, National Institutes for Quantum and Radiological Science and Technology, Chiba-shi, Japan

### ABSTRACT

The effects of a magnetic field longitudinal to the ion beam track on the generation of hydroxyl radicals ( $\bullet\text{OH}$ ) and hydrogen peroxide ( $\text{H}_2\text{O}_2$ ) in water were investigated. A longitudinal magnetic field was reported to enhance the biological effects of the ion beam. However, the mechanism of the increased cell death by a longitudinal magnetic field has not been clarified. The local density of  $\bullet\text{OH}$  generation was estimated by a method based on the EPR spin-trapping. A series of reaction mixtures containing varying concentrations (0.76–2278 mM) of DMPO was irradiated by 16 Gy of carbon- or iron-ion beams at the Heavy-Ion Medical Accelerator in Chiba (HIMAC, NIRS/QST, Chiba, Japan) with or without a longitudinal magnetic field (0.0, 0.3, or 0.6 T). The DMPO-OH yield in the sample solutions was measured by X-band EPR and plotted versus DMPO density.  $\text{O}_2$ -dependent and  $\text{O}_2$ -independent  $\text{H}_2\text{O}_2$  yields were measured. An aliquot of ultra-pure water was irradiated by carbon-ion beams with or without a longitudinal magnetic field. Irradiation experiments were performed under air or hypoxic conditions.  $\text{H}_2\text{O}_2$  generation in irradiated water samples was quantified by an EPR spin-trapping, which measures  $\bullet\text{OH}$  synthesized from  $\text{H}_2\text{O}_2$  by UVB irradiation. Relatively sparse  $\bullet\text{OH}$  generation caused by particle beams in water were not affected by loading a magnetic field on the beam track.  $\text{O}_2$ -dependent  $\text{H}_2\text{O}_2$  generation decreased and oxygen-independent  $\text{H}_2\text{O}_2$  generation increased after loading a magnetic field parallel to the beam track. Loading a magnetic field to the beam track made  $\bullet\text{OH}$  generation denser or made dense  $\bullet\text{OH}$  more reactive.

### ARTICLE HISTORY

Received 14 January 2021  
Revised 3 August 2021  
Accepted 16 August 2021

### KEYWORDS

Magnetic field; ion beam; reactive oxygen species; hydroxyl radical; hydrogen peroxide; electron paramagnetic resonance spin-trapping technique

### Introduction


It was previously reported that loading a magnetic field parallel to the particle beam track enhances the biological effects, i.e. cell lethality, of the particle beam [1–3]. However, a magnetic field loaded perpendicular to the beam track had no effect on cell death [4,5]. Applying the magnetic field after irradiation did not increase cell death [1]. The mechanism of the enhanced cell death by loading a longitudinal magnetic field on the beam track has not been clarified.

As the effects of the longitudinal magnetic field on the track were observed only during irradiation, the

mechanism must be related to the process of ionization, i.e. generation of initial reactive species, or the reactions of short lived reactive species. Effects on the ionization process may have resulted from the track structure, and/or yields of initial and secondary species. Effects on the reactivity of initial species may have resulted from the yields of secondary species.

Effects of the longitudinal magnetic field on the track structure of the particle beam may be of interest. The track structure of particle beams consists of core and penumbra regions [6]. A sequence of initial ionization on the straight linear track of the ion particle itself

**CONTACT** Ken-ichiro Matsumoto  [matsumoto.kenichiro@qst.go.jp](mailto:matsumoto.kenichiro@qst.go.jp)  Quantitative RedOx Sensing Group, Department of Radiation Regulatory Science Research, National Institute of Radiological Sciences, Quantum Life and Medical Science Directorate, National Institutes for Quantum and Radiological Science and Technology, 4-9-1 Anagawa, Inage-ku, Chiba 263-8555, Japan

 Supplemental data for this article can be accessed [here](#).

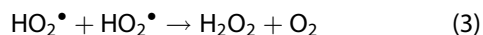
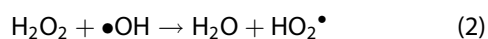
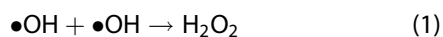
© 2021 The Author(s). Published by Informa UK Limited, trading as Taylor & Francis Group.

This is an Open Access article distributed under the terms of the Creative Commons Attribution-NonCommercial-NoDerivatives License (<http://creativecommons.org/licenses/by-nc-nd/4.0/>), which permits non-commercial re-use, distribution, and reproduction in any medium, provided the original work is properly cited, and is not altered, transformed, or built upon in any way.

makes the cylindrical core. Thus, the core is a string of overlapped spurs, as described in the spur model [7]. Higher LET particles cause denser ionization in the core, i.e. shorter interspacing of spurs. Congested ionization in the core can directly and/or indirectly cause clustered damage on DNA [8]. On the other hand, energetic secondary electrons ( $\delta$ -rays) released by the primary particle formed the penumbra region surrounding the core. Ionization caused in the penumbra region maybe sparser, like photon radiation, i.e. yielding well separated spurs in the spur model. Larger effects of particle radiation may be expected if the longitudinal magnetic field may make ionization denser or prevent the penumbra structure from spreading far from the core.

Hydroxyl radicals ( $\bullet\text{OH}$ ) are one of the initial reactive species caused by water radiolysis.  $\bullet\text{OH}$  is considered the most reactive ROS and the major player in the biological effects of ionizing radiation. Two different localized densities of  $\bullet\text{OH}$  generation were previously reported [9,10]: milli-molar level (relatively sparse) and molar level (markedly dense) generation. The intermolecular distance of the relatively sparse  $\bullet\text{OH}$  generation was estimated to be 4.3–6.6 nm and that of the markedly dense  $\bullet\text{OH}$  was assumed to be less than 1 nm. In the case of particle-beams, the relatively sparse and markedly dense  $\bullet\text{OH}$  generation may be caused in the penumbra and core regions of its beam track, respectively.

The sparsely generated  $\bullet\text{OH}$  cannot react with each other due to their distance. However, markedly dense  $\bullet\text{OH}$  generation enables the reactions of two or more  $\bullet\text{OH}$ . Reaction of two  $\bullet\text{OH}$  gives hydrogen peroxide ( $\text{H}_2\text{O}_2$ ) directly (Equation (1)). In addition,  $\text{H}_2\text{O}_2$  and  $\bullet\text{OH}$  can react to give hydroperoxyl radicals ( $\text{HO}_2^\bullet$ ) and  $\text{H}_2\text{O}$  (Equation (2)). Then,  $\text{H}_2\text{O}_2$  can be produced again by the reaction of two  $\text{HO}_2^\bullet$  (Equation (3)):



Therefore, markedly dense  $\bullet\text{OH}$  generation enables oxygen-independent  $\text{H}_2\text{O}_2$  generation.

In this study, the effects of a magnetic field-loaded parallel to the ion beam track on the ROS generation in water were investigated. Sparse  $\bullet\text{OH}$  generation, which is caused in the penumbra region of the beam track, was measured. In addition, the  $\text{O}_2$ -independent  $\text{H}_2\text{O}_2$  generation, which only occurs after markedly dense  $\bullet\text{OH}$  generation, i.e.  $\bullet\text{OH}$  generation in the core region of the beam track, was measured. The density of  $\bullet\text{OH}$  generation was discussed.

## Materials and methods

### Chemicals

5,5-Dimethyl-1-pyrroline-*N*-oxide (DMPO) was purchased from Dojindo Laboratories, Ltd. (Kumamoto, Japan). 5-(2,2-Dimethyl-1,3-propoxycyclophosphoryl)-5-methyl-1-pyrroline-*N*-oxide (CYPMPO) was a gift from Mr Masato Kamibayashi (Kyoto Pharmaceutical University at the time when the compound was gifted) [11]. Thirty percent of  $\text{H}_2\text{O}_2$  solution was purchased from FUJIFILM Wako Pure Chemical Corporation (Osaka, Japan). Other chemicals were of analytical grade. Deionized water (deionization by the Milli-Q system, Merck Millipore, Billerica, MA) was used for all experiments.

### Estimation of the density of $\bullet\text{OH}$ generation

The theory and procedures were described previously [9,10,12], and slightly modified and improved. A series of reaction mixtures of different concentrations (0.76, 1.25, 1.66, 2.28, 3.24, 4.84, 13.3, 61.5, 208, 605, 961, and 2278 mM) of DMPO was prepared using 100 mM phosphate buffer containing 0.05 mM DTPA as the solvent. The DMPO solution was then transferred to a polyethylene bag for irradiation. Then, the samples were irradiated by 16 Gy of carbon- or iron-ion beams. Hereafter, Gy means the dose that can be measured physically *via* the ion chamber. The irradiated sample was used for EPR measurement, and drawn into PTFE tubing (i.d.  $0.32 \pm 0.001$  inches, wall  $0.002 \pm 0.0005$  inches; ZEUS, Orangeburg, SC) and placed into the TE-mode EPR cavity. The EPR spectrum of DMPO-OH generated in the reaction mixture was measured using an X-band EPR spectrometer within 10 min after irradiation. For DMPO-OH, the second peak from the lower field of a 4-line spectrum was recorded. The acquired EPR spectra were analyzed using an in-house line fitting program and the Gaussian line shape was fitted. The signal height and line width of the fitted Gaussian line were measured, and the EPR signal intensity was obtained as (signal height)  $\times$  (line width)<sup>2</sup>.

The EPR signal intensity of DMPO-OH was converted to the radical concentration by comparing the signal intensity of 1 mM TEMPOL water solution as a standard. The decay rate,  $k_{\text{EXP}}$ , of DMPO-OH after irradiation was previously estimated by X-ray irradiation experiments (Supplementary Figure 1(A)). The concentration of DMPO-OH at the end of ion beam irradiation (time = 0),  $C_{0\text{EXP}}$ , was obtained by extrapolating the experimental decay curve of DMPO-OH to time = 0.

To calculate the net amount of DMPO-OH generated during ion beam irradiation,  $C_{\text{ONET}}$ , the linear generation of DMPO-OH was corrected considering the decay of DMPO-OH during ion beam irradiation (Supplementary Figure 1(B)). First,  $C_{\text{OEXP}}$  was used as the initial estimation value of  $C_{\text{ONET}}$ . The ion beam irradiation time,  $T_{\text{irrad}}$ , was divided by arbitrary least time windows ( $\Delta t_{\text{irrad}}$ ). The linear increase in DMPO-OH during  $\Delta t_{\text{irrad}}$  was  $\Delta C = C_{\text{ONET}}/T_{\text{irrad}} \times \Delta t_{\text{irrad}}$ . When the decay of DMPO-OH during ion beam irradiation was eliminated, the concentration of DMPO-OH,  $C_{\text{ti}}$ , increased by  $\Delta C$  with every  $\Delta t_{\text{irrad}}$ . The initial value of  $C_{\text{ti}}$  must be 0 at the start of irradiation ( $t_{\text{irrad}0}$ ).  $C_{\text{ti}}$  increased only by  $\Delta C$  at the first time point ( $t_{\text{irrad}1}$ ). According to the previous observation in an X-ray experiment,  $C_{\text{ti}}$  decreased during  $\Delta t_{\text{irrad}}$  at the decay rate  $k_{\text{IRD}} = 3 \times k_{\text{EXP}}$ , as described below. At the next time point ( $t_{\text{irrad}2}$ ),  $C_{\text{ti}}$  again increased by  $\Delta C$  and decayed according to  $k_{\text{IRD}}$ . By repeating this increasing and decreasing process, the corrected generation of DMPO-OH during ion beam irradiation,  $C_{\text{OSIM}}$ , was calculated.

This repeating derivative process is a combination of a zero order increasing with the rate  $C_{\text{ONET}}/T_{\text{irrad}}$  and first-order decay with the decay rate  $k_{\text{IRD}}$  simultaneously running. The time course of  $C_{\text{ti}}$  can be simplified as

$$C_{\text{ti}} = C_{\text{ONET}}/T_{\text{irrad}}/k_{\text{IRD}} \times (1 - \text{EXP}(-k_{\text{IRD}} \times t_{\text{irrad}})) \quad (4)$$

therefore,  $C_{\text{ti}}$  at the end of irradiation will be

$$C_{\text{OSIM}} = C_{\text{ONET}}/T_{\text{irrad}}/k_{\text{IRD}} \times (1 - \text{EXP}(-k_{\text{IRD}} \times T_{\text{irrad}})). \quad (5)$$

When  $C_{\text{OSIM}}$  is equal to  $C_{\text{OEXP}}$ ,  $C_{\text{ONET}}$  will be given as

$$C_{\text{ONET}} = C_{\text{OEXP}} \times T_{\text{irrad}} \times k_{\text{IRD}} / (1 - \text{EXP}(-k_{\text{IRD}} \times T_{\text{irrad}})). \quad (6)$$

Decay correction was performed on Microsoft Excel 2010.

The irradiation time,  $T_{\text{irrad}}$ , depends on both the dose rate (Gy/min) and the selected rectangle area ( $\text{cm}^2$ ) irradiated. The  $T_{\text{irrad}}$  for 16 Gy was 7–8 min for either carbon- or iron-ion beams. Irradiated DMPO water solution samples were immediately brought to the X-band EPR spectrometer and measured 4–10 min after irradiation. The  $k_{\text{EXP}}$  value previously observed by X-ray experiments varied depending on the DMPO concentration in the sample solution (Supplementary Figure 2).

The estimated net concentration of DMPO-OH in the irradiated sample solutions was plotted versus the density of DMPO in the sample solution. The DMPO density, which was defined as the number of DMPO molecules aligned on the linear unit distance, is the reciprocal of the inter-molecular distance of DMPO molecules at a certain concentration. The density of  $\bullet\text{OH}$

was estimated from the inflection point of the plot profile.

### Estimation of the decay rate of DMPO-OH during irradiation

The 2278 mM water solutions of DMPO were irradiated at several different doses (8, 16, 32, and 64 Gy) of X-rays at a constant dose rate (3 Gy/min). Estimated net DMPO-OH yields,  $C_{\text{ONET}}$ , in the sample solutions were plotted with the X-ray dose (Supplementary Figure 3). The linearity between X-ray dose and  $C_{\text{ONET}}$  was estimated by the  $R^2$  value of linear regression, and the  $k_{\text{IRD}}$  value was adjusted to achieve the maximum  $R^2$  value. The best linearity between  $C_{\text{ONET}}$  and X-ray dose was observed when  $k_{\text{IRD}} = 3.05 \times k_{\text{EXP}}$ . This value was used for decay correction in this paper.

### Measurement of $\text{O}_2$ -dependent and $\text{O}_2$ -independent $\text{H}_2\text{O}_2$ yields

Experiments were performed under aerobic or hypoxic (<0.1% oxygen) conditions. For irradiation under aerobic conditions, 350  $\mu\text{l}$  of milli-Q water was sealed in an  $\text{O}_2$ -permeable polyethylene bag. For hypoxic experiments, the sample sealed in the polyethylene bag was moved into a glove box and  $\text{N}_2$  gas was pumped in to establish a 0.5% or lower  $\text{O}_2$  atmosphere. The polyethylene bag containing the sample solution was again sealed in an  $\text{O}_2$ -impermeable bag with an  $\text{O}_2$ -absorber and colorimetric  $\text{O}_2$ -marker (Supplementary Figure 4). The  $\text{O}_2$ -impermeable bag, oxygen absorber, and oxygen indicator were purchased from I.S.O. Inc. (Yokohama, Japan). The oxygen marker remained pink in color under a hypoxic (<0.1%  $\text{O}_2$ ) atmosphere, but changed to bluish-violet when it sensed oxygen. The change in color of the  $\text{O}_2$ -marker is reversible.

The samples were irradiated by 32 Gy in the carbon-ion beam experiment and 64 Gy in the iron-ion beam experiment.  $\text{H}_2\text{O}_2$  yields were expected to become lower than  $\bullet\text{OH}$  yields and to decrease with increasing LET under aerobic conditions, as reported previously [10]. In addition,  $\text{O}_2$ -independent  $\text{H}_2\text{O}_2$  yields,  $\text{H}_2\text{O}_2$  yields under hypoxic conditions, were expected to be lower than those under aerobic conditions. Therefore a higher dose, 32 Gy, was selected in the  $\text{H}_2\text{O}_2$  detection experiment than in the  $\bullet\text{OH}$  detection experiment. An additional higher dose, 64 Gy, was selected for iron-ion beams, which have a higher LET than carbon-ion beams.

$\text{H}_2\text{O}_2$  was detected and quantified by the UV method [13]. The UV method detects  $\bullet\text{OH}$  synthesized from

H<sub>2</sub>O<sub>2</sub> by UVB irradiation of the water sample. The •OH was trapped by DMPO and then DMPO-OH was measured as an index of H<sub>2</sub>O<sub>2</sub> using X-band EPR. A 90- $\mu$ l aliquot of the irradiated water sample was taken into a micro-tube, and 10  $\mu$ l of 1 M DMPO water solution was added into the micro-tube and then mixed. The water sample was irradiated by UVB (12,000  $\mu$ W/cm<sup>2</sup>) for 5 min. Immediately after UVB irradiation, the water sample was drawn into PTFE tubing and placed into the TE-mode EPR cavity. X-band EPR spectra were measured repeatedly 13 times every 30 s, i.e. for 6 min. The amount of H<sub>2</sub>O<sub>2</sub> generated per dose was estimated using a standard curve previously prepared using a series of H<sub>2</sub>O<sub>2</sub> water solutions of known concentrations (4.9–29.4  $\mu$ M).

### **X-band EPR measurement**

The PTFE tubing holding 100  $\mu$ l of sample solution was set in a TE-mode EPR cavity using a quartz sample tube and then measured using an X-band EPR spectrometer (JEOL, Tokyo, Japan). EPR data acquisition was controlled by the WIN-RAD ESR Data Analyzer System (Radical Research, Inc., Hino, Tokyo, Japan). EPR conditions were as follows: microwave frequency, 9.4 GHz; microwave power, 2.00 mW; lower magnetic field, 335.5 mT; field sweep width: +0.75 mT, sweep time: 15 s, data resolution: 1024 points; field modulation frequency, 100 kHz; field modulation amplitude, 0.063 mT; time constant, 0.01 s.

### **Ion beam irradiation**

Ion beam irradiation of the sample was performed at the Heavy-Ion Medical Accelerator in Chiba (HIMAC, National Institute of Radiological Sciences, Chiba, Japan). Experiments were performed using the experimental scanning beam line (SB1). The polyethylene bag containing the reaction mixture was attached to a flat acrylic sample holder and set at the center of the solenoid magnet on the isocenter of the beam. The sample was irradiated by carbon or iron ions accelerated to 350 MeV/nucleon at room temperature. A uniform 3.2  $\times$  3.2-cm<sup>2</sup> field for •OH detection or 4.8  $\times$  3.2-cm<sup>2</sup> field for H<sub>2</sub>O<sub>2</sub> detection at the isocenter plane was irradiated by scanning a narrowly focused ionbeam. A narrow pencil beam can scan uniformly in the selected area [14]. The irradiated field (rectangle area) was tailored to the sample size and number of samples. The irradiated field should be slightly larger than the actual sample size for irradiating samples. Single-packed DMPO solution samples were irradiated for •OH

detection. Double-packed water samples under aerobic and hypoxic conditions were simultaneously irradiated for H<sub>2</sub>O<sub>2</sub> detection. The LET at the surface of the sample for the carbon-ion beam irradiation was 12 keV/ $\mu$ m and that for the iron-ion beam was 222 keV/ $\mu$ m. Irradiation was performed with or without a magnetic field loaded longitudinal to the beam track.

### **Loading a magnetic field parallel to the beam track**

A water-cooled solenoid magnet with a bore of 10.5 cm in diameter and 16.8 cm in length was positioned at the isocenter to produce a homogeneous magnetic field longitudinal to the ion beams. Details of magnet settings are described previously [2,3]. The magnetic field strength loaded was switched at 0, 0.3, or 0.6 T.

### **Statistical analysis**

Statistical differences were estimated using the TTEST function in Microsoft Excel 2010. Suitable “tail” and “type” for the TTEST function were selected as follows: the “tail” was 2 (two-tailed distribution) for stability tests because the difference between the two data groups was compared simply. The “type” was selected according to the equality of variances between the data sets, which was estimated using the FTEST function. Grades of significance were estimated by  $p < 0.05$ ,  $p < 0.01$ , and  $p < 0.001$ .

### **Results and discussion**

The results of density estimation of •OH generation in water irradiated by carbon-ion beams are shown in Figure 1. The plot of DMPO-OH yields in the irradiated sample solution versus DMPO density in the sample solution exhibited a typical 3-phase profile. The generation of sparse •OH can be estimated from the inflection point of the first phase and the second phase. The density of •OH generated under no magnetic field (Figure 1(A)) was estimated as 146  $\mu$ m<sup>-1</sup>, which was converted to 6.8 nm as the intermolecular distance and 5.2 mM as the local concentration. The results observed under a 0.3- or 0.6-T longitudinal magnetic field are shown in Figure 1(B,C), respectively. The density of sparse •OH generated under a 0.3 and 0.6-T longitudinal magnetic field (Figure 1(B,C)) was estimated as 154 and 156  $\mu$ m<sup>-1</sup>, which was converted to 6.5 and 6.4 nm as the intermolecular distance, and 6.1 and 6.4 mM as the local concentration, respectively. The yields of DMPO-OH estimated at the inflection point,

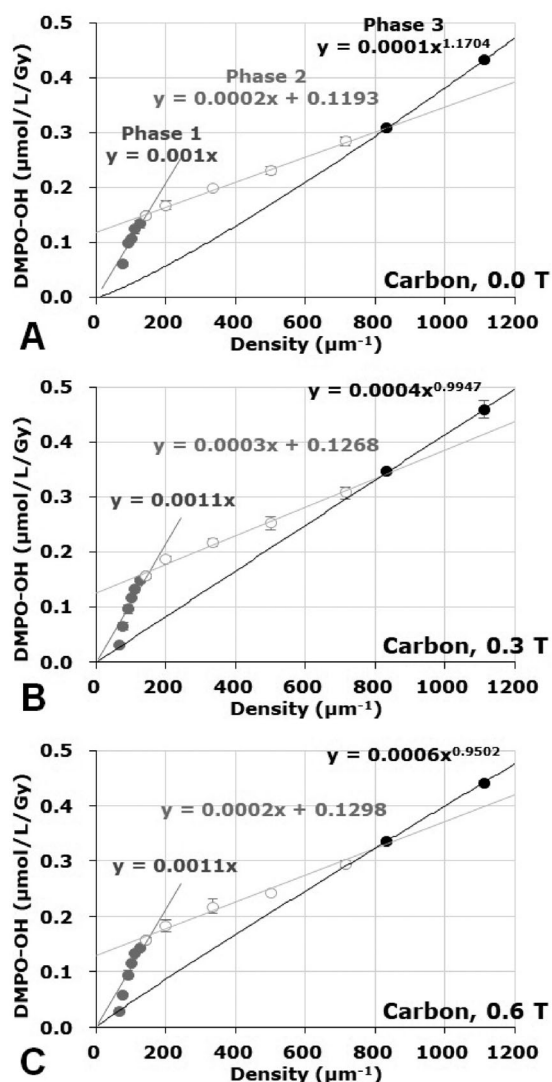


**Figure 1.** Estimation of the density of  $\bullet\text{OH}$  generation in water irradiated by carbon-ion beams. Concentrations of DMPO-OH generated in the reaction mixture irradiated by carbon-ion beams were plotted versus the density of the DMPO in the corresponding reaction mixture. Experiments were performed under a (A) 0.0-T, (B) 0.3-T, or (C) 0.6-T longitudinal magnetic field loaded on the beam track. Marks and the error bars indicate the average and SD of three measurements. Plots showed a characteristic 3-phase profile.

which were considered as sparse OH yields, were 0.16, 0.17, and 0.17  $\mu\text{mol/L/Gy}$  in the experiments under 0.0-, 0.3-, and 0.6-T longitudinal magnetic fields, respectively. Maximum DMPO-OH yields observed in 2.3 M ( $1111 \mu\text{m}^{-1}$ ) DMPO solutions were 0.43, 0.46, and 0.44  $\mu\text{mol/L/Gy}$  under 0.0-, 0.3-, and 0.6-T longitudinal magnetic fields, respectively.

The results of density estimation of  $\bullet\text{OH}$  generation in water irradiated by iron-ion beams are shown in Figure 2. The height of the inflection point made by the first phase and the second phase was lower than that

of the corresponding height observed with carbon-ion beams. The yields of DMPO-OH estimated at the inflection point were 0.094, 0.099, and 0.099  $\mu\text{mol/L/Gy}$  in the experiments under 0.0-, 0.3-, and 0.6-T longitudinal magnetic fields, respectively. However, the densities of sparse  $\bullet\text{OH}$  generated were similar to those in carbon-ion beam experiments, being 160, 160, and 157  $\mu\text{m}^{-1}$  under 0.0-, 0.3-, and 0.6-T longitudinal magnetic fields, respectively. Maximum DMPO-OH yields observed in 2.3 M DMPO solutions were 0.37, 0.37, and 0.41  $\mu\text{mol/L/Gy}$  under 0.0-, 0.3-, and 0.6-T longitudinal magnetic fields, respectively.

The sparse  $\bullet\text{OH}$  generation in water irradiated by iron-ion beams becomes lower than that by carbon-ion beams. This is consistent with a previous paper [9] that reported that sparse  $\bullet\text{OH}$  generation became lower with increasing LET of carbon-ion beams. However, loading of a longitudinal magnetic field had little effect on the density of sparse  $\bullet\text{OH}$  generation or on the yield of sparse  $\bullet\text{OH}$ . The sparse  $\bullet\text{OH}$  generation is mainly caused in the penumbra region. The effects of the longitudinal magnetic field on the dense  $\bullet\text{OH}$  generation was unable to be evaluated from the plots shown in Figures 1 and 2.

To estimate the actual value (intermolecular distance or density) for dense  $\bullet\text{OH}$ , the inflection point formed by the third and the fourth phase has to be observed. However, quantitative measurement of DMPO-OH in a high-concentration DMPO solution beyond 2 M is difficult due to variation of permittivity of the sample solution, which can alter hyperfine splitting, i.e. the signal shape, and the sensitivity of the EPR detector. As the experiments described in this paper were able to observe only the first, second, and third phases, the actual value for dense  $\bullet\text{OH}$  was unable to be obtained. Only the existence of dense  $\bullet\text{OH}$  in this stage is known.

The decay of DMPO-OH after irradiation may be due to spontaneous one-electron reduction, and the oxygen may reoxidize it. As the decay of DMPO-OH after irradiation is slightly faster under a hypoxic atmosphere, dissolved oxygen in the reaction mixture may make it slower (data not shown). An additional reduction may have occurred during irradiation because the decay rate of DMPO-OH during irradiation,  $k_{\text{IRD}}$ , was expected to be faster than that after irradiation,  $k_{\text{EXP}}$ . Stable nitroxyl radicals, TEMPOL and carbamoyl-PROXYL, were reduced during X-ray irradiation [12]. In addition, highly concentrated  $\text{H}_2\text{O}_2$  clusters are likely related to this reduction mechanism of nitroxyl radicals [12]. DMPO-OH is a nitroxyl radical, but it is not completely stable like TEMPOL and/or PROXYL compounds. Therefore, DMPO-OH may undergo decay by the highly

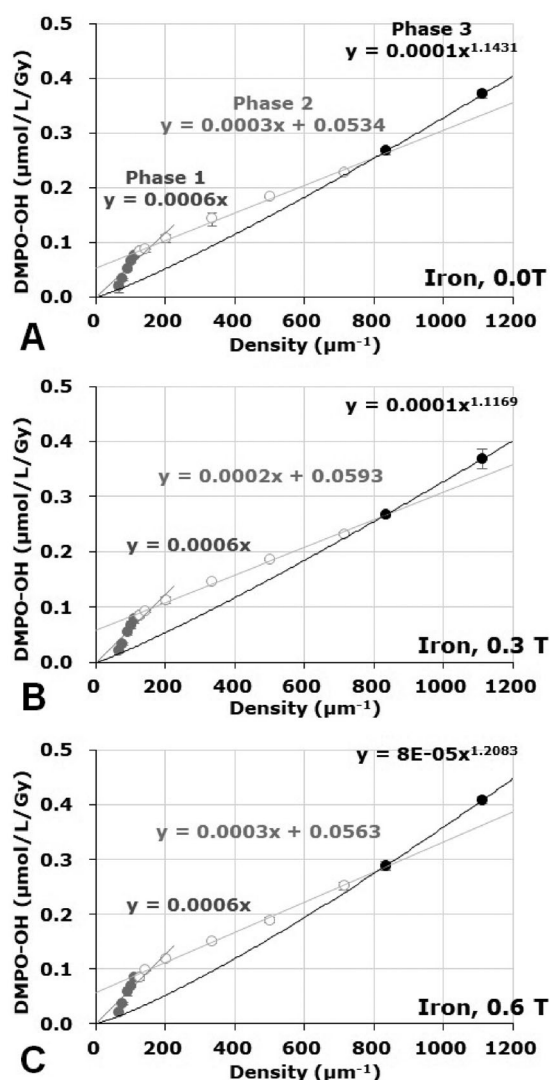


**Figure 2.** Density estimation of  $\bullet\text{OH}$  in water irradiated by iron-ion beams with or without a longitudinal magnetic field loaded on the beam track. Concentrations of DMPO-OH generated in the reaction mixture irradiated by carbon-ion beams were plotted versus the density of the DMPO in the corresponding reaction mixture. Experiments were performed under a (A) 0.0-T, (B) 0.3-T, or (C) 0.6-T longitudinal magnetic field loaded on the beam track. Marks and the error bars indicate the average and SD of three measurements. Plots showed a characteristic 3-phase profile.

concentrated  $\text{H}_2\text{O}_2$  cluster during X-ray irradiation similar to TEMPOL and carbamoyl-PROXYL.

To accurately estimate the  $\bullet\text{OH}$  yield, mathematical correction of the decay rate of DMPO-OH was introduced [9] and modified to calculate the true value. In this report, the decay rate of DMPO-OH during irradiation,  $k_{\text{IRD}}$ , was corrected by a factor of 3.05, which was observed in the experiment shown in [Supplementary Figure 3](#). The reduction rate of DMPO-OH during irradiation must be assessed, but it was unable to be measured directly. The experiment was thus carried out

using several different doses (8, 16, 32, and 64 Gy) at a constant dose rate (3 Gy/min). Therefore, the irradiation time,  $T_x$ , varied depending on the dose, i.e. 2 min 40 s, 5 min 20 s, 10 min 40 s, and 21 min 20 s for 8, 16, 32, and 64 Gy, respectively. The results of this experiment are shown in [Supplementary Figure 3](#). A longer irradiation time yielded a lower estimation, which is why the decay rate of DMPO-OH during irradiation,  $k_{\text{IRD}}$ , was estimated to be slower.

The correction factor for  $k_{\text{IRD}}$  may vary depending on the dose rate because the decay of DMPO-OH during irradiation may depend on highly concentrated  $\text{H}_2\text{O}_2$  clusters and the  $\bullet\text{OH}$  yield during irradiation. A higher dose rate may lead to the faster decay of DMPO-OH during irradiation. Therefore, suitable factors are required to accurately quantify the  $\bullet\text{OH}$  yield induced by X-ray or carbon-ion beam irradiation at different dose rates. In particular, particle beams yield different dose rates depending on the LET of the beam. However, accurate  $\bullet\text{OH}$  quantification is not required to describe the effects of magnetic fields, which were compared among identical dose rates in this study.

The  $\text{H}_2\text{O}_2$  yield in the water irradiated by carbon-ion beams with or without loading of a longitudinal magnetic field is shown in [Figure 3\(A\)](#). The yield of  $\text{H}_2\text{O}_2$  under aerobic conditions was significantly reduced by longitudinal 0.6-T magnetic fields; however, it only slightly increased or remained the same with a 0.3-T magnetic field. The yield of  $\text{H}_2\text{O}_2$  under hypoxic conditions was significantly increased by longitudinal 0.3- and 0.6-T magnetic fields in an intensity-dependent manner. The  $\text{H}_2\text{O}_2$  yield under aerobic conditions corresponds to the total  $\text{H}_2\text{O}_2$  generation. The  $\text{H}_2\text{O}_2$  yield under hypoxic conditions corresponds to  $\text{O}_2$ -independent  $\text{H}_2\text{O}_2$  generation. The difference between the aerobic and hypoxic  $\text{H}_2\text{O}_2$  yields corresponds to  $\text{O}_2$ -dependent  $\text{H}_2\text{O}_2$  generation, which significantly decreased by loading longitudinal magnetic fields in an intensity-dependent manner.

The  $\text{H}_2\text{O}_2$  yield in the water irradiated by iron-ion beams is shown in [Figure 3\(B\)](#). The iron-ion beams produced a lower yield of aerobic  $\text{H}_2\text{O}_2$  and higher yield of hypoxic  $\text{H}_2\text{O}_2$  than carbon-ion beams under no magnetic field. The yields of  $\text{H}_2\text{O}_2$  under aerobic conditions were significantly reduced by a longitudinal 0.6-T magnetic field. The yields of  $\text{H}_2\text{O}_2$  under hypoxic conditions did not change after loading a magnetic field, but relatively higher values were maintained. The  $\text{O}_2$ -dependent  $\text{H}_2\text{O}_2$  generation was significantly reduced by loading magnetic fields in an intensity-dependent manner.

In aerobic conditions,  $\text{H}_2\text{O}_2$  generation by lower LET beams is mainly associated with oxygen consumption

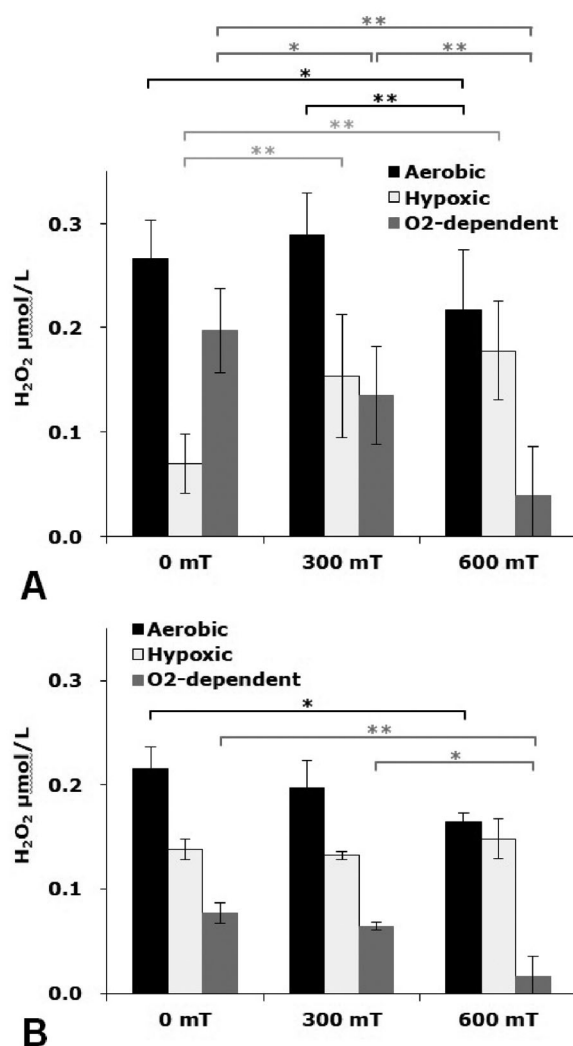
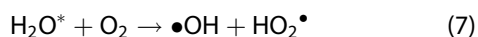


**Figure 3.** Effects of a longitudinal magnetic field on the H<sub>2</sub>O<sub>2</sub> yields in water irradiated by ion beams. (A) H<sub>2</sub>O<sub>2</sub> yields in water irradiated by carbon-ion beams. (B) H<sub>2</sub>O<sub>2</sub> yields in water irradiated by iron-ion beams. Black columns indicate H<sub>2</sub>O<sub>2</sub> yield under aerobic conditions, which corresponds to the total H<sub>2</sub>O<sub>2</sub> generation. Light gray columns indicate H<sub>2</sub>O<sub>2</sub> yield under hypoxic conditions, which corresponds to O<sub>2</sub>-independent H<sub>2</sub>O<sub>2</sub> generation. Dark gray columns indicate the O<sub>2</sub>-dependent H<sub>2</sub>O<sub>2</sub> generation, which was estimated by subtraction of the H<sub>2</sub>O<sub>2</sub> yield under hypoxic conditions of each measurement from the average total H<sub>2</sub>O<sub>2</sub> yields under the same magnetic field condition. \* and \*\* indicates significance with  $p < 0.05$  and  $p < 0.01$ , respectively.

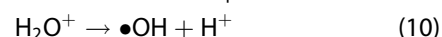
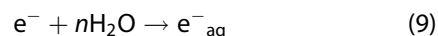
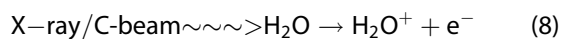
[10]. During rapid O<sub>2</sub>-dependent H<sub>2</sub>O<sub>2</sub> generation, HO<sub>2</sub><sup>•</sup> is generated by the reaction of a hydrogen radical (•H) and O<sub>2</sub> [Equation (6)], or by reaction of excited water (H<sub>2</sub>O\*) and O<sub>2</sub> [Equation (7)]. Then, 2 HO<sub>2</sub><sup>•</sup> react to give H<sub>2</sub>O<sub>2</sub> [Equation (3)]:



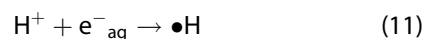
This is associated with sparse ionization, which occurred in the penumbra region of the track. Both •H

and •OH were generated from ionized or excited water; however, the sparsely generated •OH cannot react with each other due to distance. Highly reactive •OH cannot move the intermolecular distance of •OH, which is over 6 nm (Figures 1 and 2). Therefore, direct H<sub>2</sub>O<sub>2</sub> generation with Equation (1) cannot occur from sparsely generated •OH. The decrease in O<sub>2</sub>-dependent H<sub>2</sub>O<sub>2</sub> generation may reflect a decrease in •H generation or increase in •H consumption/cancellation. The increasing O<sub>2</sub>-independent H<sub>2</sub>O<sub>2</sub> generation, H<sub>2</sub>O<sub>2</sub> generation under hypoxic conditions, may simply be due to an increase in dense •OH due to increasing dense ionization. Thus, the cancellation of •H, i.e. reaction of •H to make H<sub>2</sub>, or reaction with •OH to make H<sub>2</sub>O will also increase.

Hydrated electrons (e<sup>-</sup><sub>aq</sub>) can be generated simultaneously with •OH through the water radio-lysis process [Equation (8)–(10)]:



Then, e<sup>-</sup><sub>aq</sub> reacts with H<sup>+</sup> to give •H [Equation (11)].



If the oxygen can react with e<sup>-</sup><sub>aq</sub> before Equation (11), O<sub>2</sub><sup>•-</sup> may be generated by Equation (12):



However, Equation (11) is dominant to Equation (12) even in aerobic conditions for the following reason:

When DMPO water solution was irradiated by X-rays or carbon-ion beams, the EPR signal of DMPO-OH and DMPO-H was observed in the irradiated solution [15,16]. For example, a time course of EPR spectra observed in 1.7 M DMPO solution irradiated by 32 Gy of carbon-ion beams is shown in Supplementary Figure 5(A). However, no trace of DMPO-OOH was observed in the DMPO water solution irradiated by either X-rays or carbon-ion beams. The decay rates of DMPO-OH and DMPO-H observed in 1.7 M DMPO water solution after X-ray irradiation, i.e.  $k_{\text{EXP}}$ , were 0.0215 and 0.1968 min<sup>-1</sup>, corresponding to a half-life of 32.2 and 3.5 min, respectively. The half-life of DMPO-OOH was reported to be around 1 min [11,17], but this short half-life is unlikely the reason for why DMPO-OOH was not observed in the irradiated DMPO water solution.

5-(2,2-Dimethyl-1,3-propoxy cyclophosphoryl)-5-methyl-1-pyrroline N-oxide (CYPMPO) is another type of spin-trapping agent. The O<sub>2</sub><sup>•-</sup> adduct of CYPMPO, i.e. CYPMPO-OOH, is much more stable than DMPO-OOH and its half-life was reported to be 15 min [11]. If the O<sub>2</sub> reacted with e<sup>-</sup><sub>aq</sub> before Equation (11), and O<sub>2</sub><sup>•-</sup> was

generated by Equation (12), CYPMPO-OOH should have been observed after X-ray or carbon-ion beam irradiation of CYPMPO water solution. However, CYPMPO-OOH was not observed after either X-ray (Supplementary Figure 6) or carbon-ion beam irradiation (data not shown) of CYPMPO water solution. There is only one report in which a CYPMPO-OOH adduct was observed after gamma-irradiation of aqueous 1.0 mM CYPMPO solution [18]; however, the reaction mixture contained 200 mM HCOOH and was bubbled by O<sub>2</sub> gas. Therefore, Equation (11) is dominant to Equation (12) in simple water solution of spin-trapping agents under aerobic conditions.

In addition, similar amounts of •H and •OH were detected by DMPO spin-trapping (Supplementary Figure 5(B)) in the reaction system used in the current study. The presence of oxygen was unable to suppress the •H detection by DMPO and a similar amount of DMPO-H was observed under aerobic and hypoxic conditions (data not shown). This suggests that O<sub>2</sub> was unable to consume e<sup>-</sup><sub>aq</sub> under aerobic conditions and that Equation (11) is the most available source of •H generation. Thus, direct one-electron reduction of O<sub>2</sub> by e<sup>-</sup><sub>aq</sub>, which gives O<sub>2</sub><sup>•-</sup>/HO<sub>2</sub><sup>•</sup>, and sequential H<sub>2</sub>O<sub>2</sub> generation are minor. The main source of O<sub>2</sub><sup>•-</sup>/HO<sub>2</sub><sup>•</sup> under aerobic conditions is probably Equation (6). Under hypoxic conditions, radiation-induced H<sub>2</sub>O<sub>2</sub> generation decreased due to O<sub>2</sub>-dependent H<sub>2</sub>O<sub>2</sub> generation through Equations (3) and (6) was suppressed [13].

The methods used for quantification of H<sub>2</sub>O<sub>2</sub> were carefully compared and we concluded that the UV method yielded good reproducibility [13]. The sample of ultrapure water (deionized by the milli-Q system) may contain only water and air (or only N<sub>2</sub> in the hypoxic sample). Irradiating the water sample by X-rays or carbon-ion beams can induce several ROS. Only H<sub>2</sub>O<sub>2</sub> will remain in the sample water after irradiation due to its stability, but other unstable ROS are canceled and/or converted to H<sub>2</sub>O<sub>2</sub>. When an aliquot of DMPO was added to the sample and the sample water was irradiated by UVB, the available sources of DMPO-OH in the irradiated sample water were UV-induced •OH generation from H<sub>2</sub>O<sub>2</sub> and UV-degradation of DMPO. However, there was only a trace yield of DMPO-OH by UV-degradation of DMPO [19] and it was not detectable in 100 mM DMPO solution used in the current study. The UV method is an effective procedure for quantifying H<sub>2</sub>O<sub>2</sub> in a simple and clear reaction system. Another advantage of the UV method is that the quantification of H<sub>2</sub>O<sub>2</sub> can be performed using relatively small sample volumes of less than 100 μl per measurement.

The three methods for quantifying H<sub>2</sub>O<sub>2</sub>, the quinoid-dye method, the Fenton method, and the UV method, were compared in the previous paper [13]. The quinoid-dye method is based on measurement of a red quinoid-dye, which has absorbance at 505 nm, formed by a reaction of 4-aminoantipyrine, phenol, and H<sub>2</sub>O<sub>2</sub> in the presence of peroxidase [20]. The Fenton method detects •OH synthesized from H<sub>2</sub>O<sub>2</sub> in the presence of Fe<sup>2+</sup> using EPR with DMPO as the spin-trapping agent [21,22]. The UV method also detects UV-induced •OH from H<sub>2</sub>O<sub>2</sub> by the EPR spin-trapping, as described above. The three methods produced similar but slightly different values; however, the same response to different LET radiation and oxygen concentrations was observed.

There are several reports of magnetic fields affecting chemical reactions [23–25]. However, this was only expected at relatively high concentrations (several millimolar to molar levels) of the reacting compounds. The local concentration of markedly dense •OH is expected to exceed 2.3 M. If such markedly dense •OH generation is sequential on the track core, this 2.3 M was only when the longitudinal direction was considered. However, in the direction perpendicular to the beam track, the next •OH should exist on another beam track, which may be separated by several mm or more (Supplementary Figure 7). When nanosecond moment is considered, even the number of incoming particles depends on the dose rate. Thus, the concentration of •OH is infinitely low (probably 10<sup>-18</sup> mol/L) when the perpendicular direction to the beam track is considered. Therefore, only the reactions of markedly dense •OH on the track can be affected by the longitudinal magnetic field.

Modification of under-nm-levels of •OH generation in water irradiated by ion beams caused by a longitudinal magnetic field on the beam track may be one reason for the increased cell death. In addition, the generation of highly concentrated H<sub>2</sub>O<sub>2</sub> clusters was expected under such highly concentrated •OH conditions [12]. H<sub>2</sub>O<sub>2</sub> can function as a strong oxidant at a high concentration. It stimulates the skin and mucosa, and 10 w/v% (~3 M) or higher H<sub>2</sub>O<sub>2</sub> solution causes white patches and pain upon contact with skin/mucosa. The volume and/or number of high-concentration H<sub>2</sub>O<sub>2</sub> clusters may also increase due to O<sub>2</sub>-independent H<sub>2</sub>O<sub>2</sub> generation.

## Conclusion

Relatively sparse •OH generation caused by particle beams in water was not affected by loading a magnetic field on the beam track. Oxygen-dependent H<sub>2</sub>O<sub>2</sub> generation decreased and oxygen-independent H<sub>2</sub>O<sub>2</sub>



generation increased after loading a magnetic field parallel to the beam track. Loading a magnetic field parallel to the beam track made  $\bullet\text{OH}$  generation denser or increased the reaction of dense  $\bullet\text{OH}$ .

## Acknowledgments

The authors are grateful to the staff of the HIMAC for their help with irradiating the samples. The authors are also grateful to Mr Masato Kamibayashi (Kyoto Pharmaceutical University at the time when the compound was gifted) for the gift of CYPMPO

## Disclosure statement

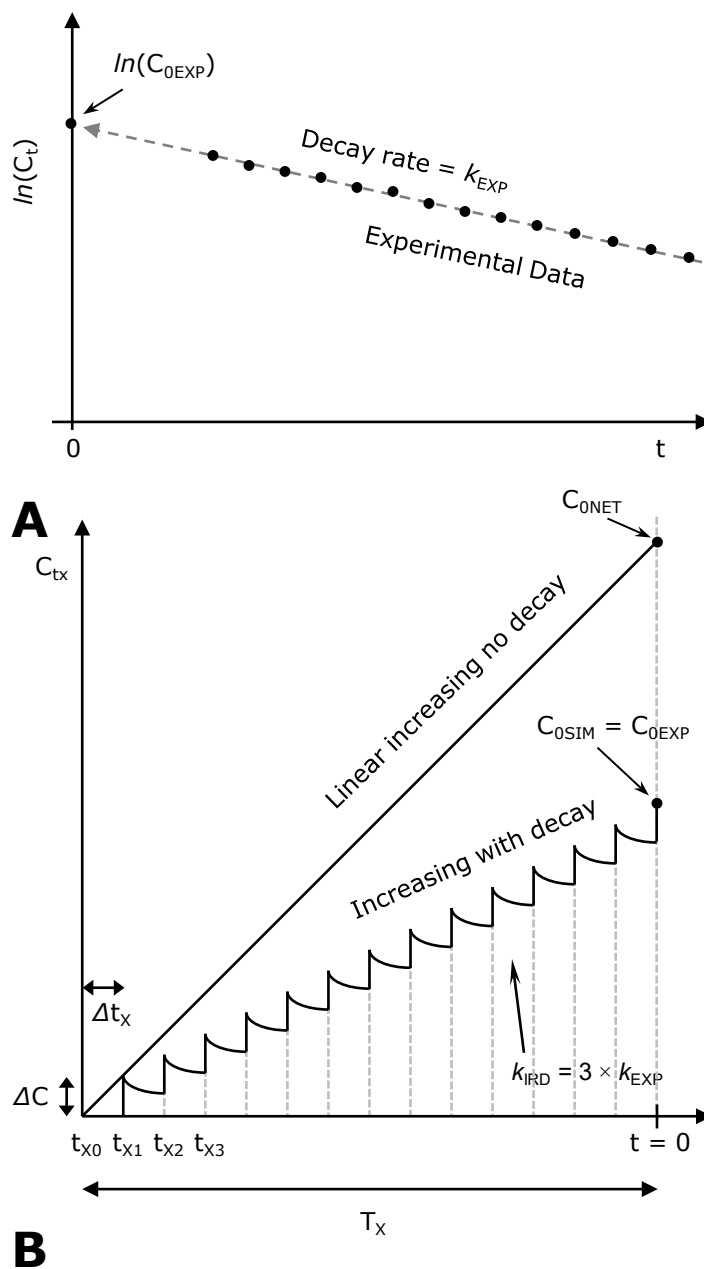
No potential conflict of interest was reported by the author(s).

## Funding

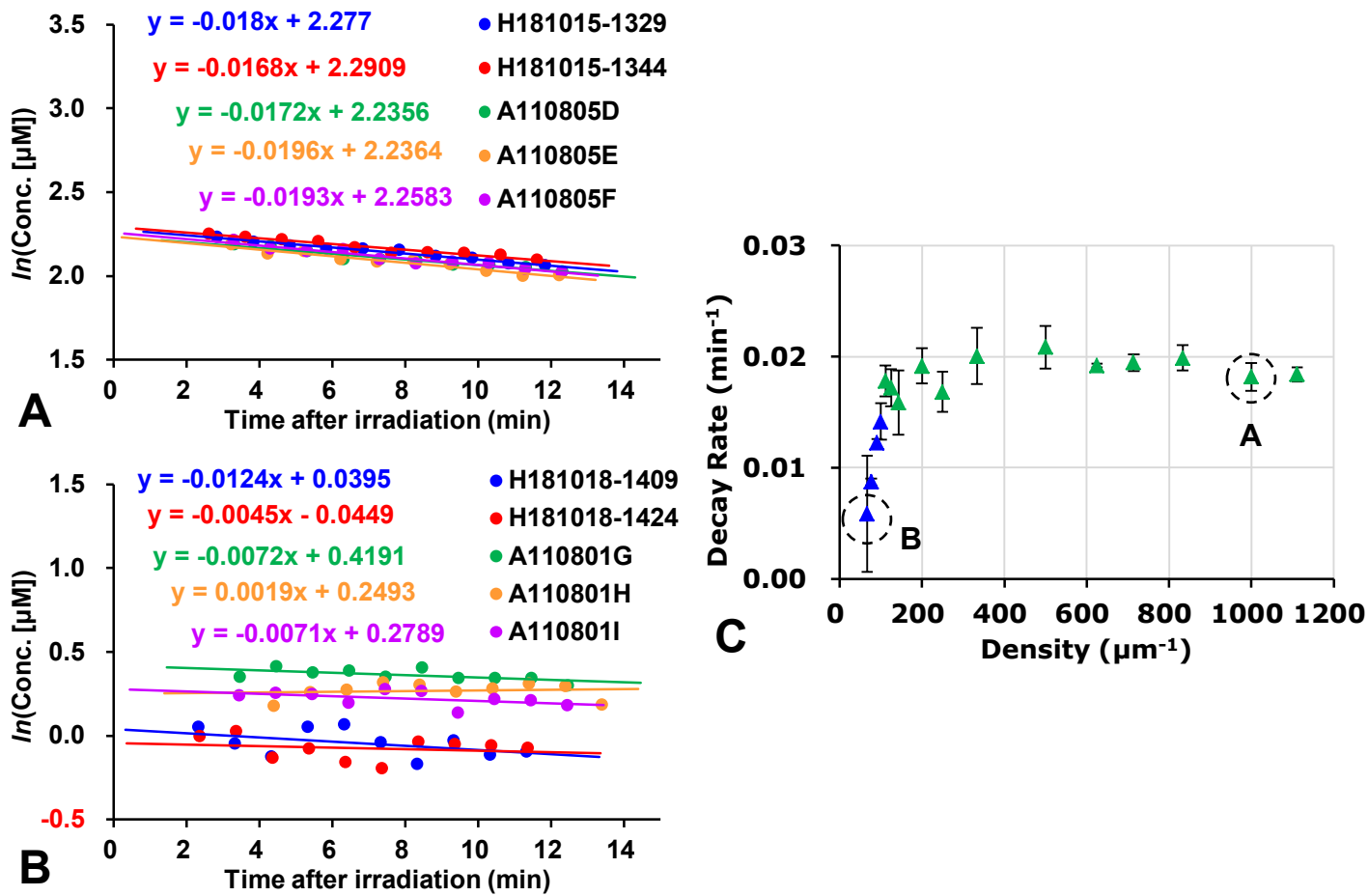
This study was partly supported by JSPS KAKENHI Grant no. 20K08123 (T.I.).

## References

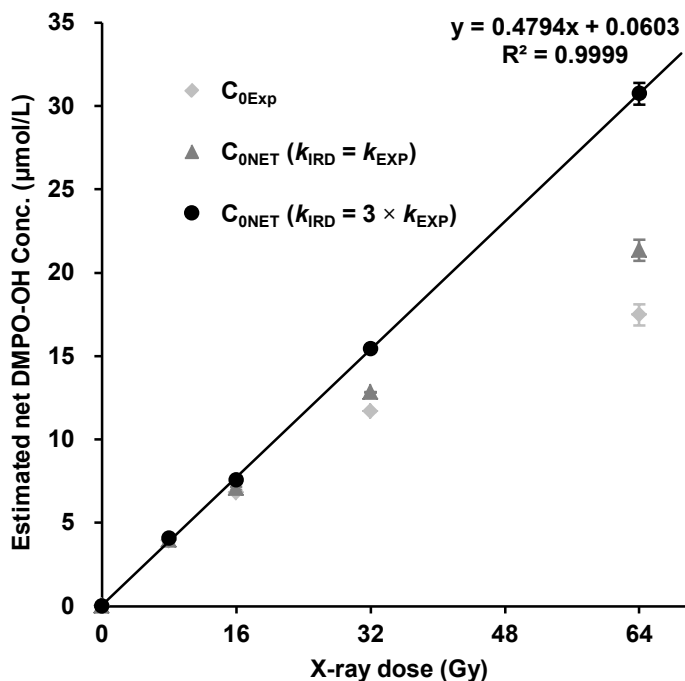
- [1] Inaniwa T, Suzuki M, Sato S, et al. Effects of magnetic field applied just before, during or immediately after carbon-ion beam irradiation on its biological effectiveness. *Radiat Res.* 2019;192(6):662–225.
- [2] Inaniwa T, Suzuki M, Sato S, et al. Enhancement of biological effectiveness of carbon-ion beams by applying a longitudinal magnetic field. *Int J Radiat Biol.* 2019;95(6):720–724.
- [3] Inaniwa T, Suzuki M, Sato S, et al. Effect of external magnetic fields on biological effectiveness of proton beams. *Int J Radiat Oncol Biol Phys.* 2020;106(3):597–603.
- [4] Inaniwa T, Suzuki M, Sato S, et al. Influence of a perpendicular magnetic field on biological effectiveness of carbon-ion beams. *Int J Radiat Biol.* 2019;95(9):1346–1350.
- [5] Yudhistiara B, Weber KJ, Huber PE, et al. Carbon ion and proton beam irradiation of a normal human TK6 lymphoblastoid cell line within a magnetic field of 1.0 tesla. *Cancer Manag Res.* 2019;11:8327–8335.
- [6] Muroya Y, Plante I, Azzam EI, et al. High-LET ion radiolysis of water: visualization of the formation and evolution of ion tracks and relevance to the radiation-induced bystander effect. *Radiat Res.* 2006;165(4):485–491.
- [7] Mozumder A, Magee JL. Model of tracks of ionizing radiations for radical reaction. *Radiat Res.* 1966;28(2):203–214.
- [8] Hagiwara Y, Oike T, Niimi A, et al. Clustered DNA double-strand break formation and the repair pathway following heavy-ion irradiation. *J Radiat Res.* 2019;60(1):69–79.
- [9] Matsumoto K, Ueno M, Nakanishi I, et al. Density of hydroxyl radicals generated in an aqueous solution by irradiating carbon-ion beam. *Chem Pharm Bull (Tokyo).* 2015;63(3):195–199.
- [10] Matsumoto K, Nyui M, Ueno M, et al. A quantitative analysis of carbon-ion beam-induced reactive oxygen species and redox reactions. *J Clin Biochem Nutr.* 2019;65(1):1–7.
- [11] Kamibayashi M, Oowada S, Kameda H, et al. Synthesis and characterization of a practically better DEPMPO-type spin trap, 5-(2,2-dimethyl-1,3-propoxy cyclophosphoryl)-5-methyl-1-pyrroline *N*-oxide (CYPMPO). *Free Radic Res.* 2006;40(11):1166–1172.
- [12] Ueno M, Nakanishi I, Matsumoto K. Generation of localized highly concentrated hydrogen peroxide clusters in water by X-rays. *Free Radic Res.* 2020;54(5):360–372.
- [13] Matsumoto K, Ueno M, Nyui M, et al. Effects of LET on oxygen-dependent and-independent generation of hydrogen peroxide in water irradiated by carbon-ion beams. *Free Radic Res.* In press. Accepted on April 7, 2021. DOI:10.1080/10715762.2021.1915489
- [14] Furukawa T, Inaniwa T, Sato S, et al. Performance of the NIRS fast scanning system for heavy-ion radiotherapy. *Med Phys.* 2010;37(11):5672–5682.
- [15] Moritake T, Tsuboi K, Anzai K, et al. ESR spin trapping of hydroxyl radicals in aqueous solution irradiated with high-LET carbon-ion beams. *Radiat Res.* 2003;159(5):670–675.
- [16] Madden KP, Taniguchi H. The role of the DMPO-hydrated electron spin adduct in DMPO- $\bullet\text{OH}$  spin trapping. *Free Radic Biol Med.* 2001;30(12):1374–1380.
- [17] Saito K, Takahashi M, Kamibayashi M, et al. Comparison of superoxide detection abilities of newly developed spin traps in the living cells. *Free Radic Res.* 2009;43(7):668–676.
- [18] Oka T, Yamashita S, Midorikawa M, et al. Spin-trapping reactions of a novel gauchetype radical trapper G-CYPMPO. *Anal Chem.* 2011;83(24):9600–9604.
- [19] Ueno M, Nakanishi I, Matsumoto K. Inhomogeneous generation of hydroxyl radicals in hydrogen peroxide solution induced by ultraviolet irradiation and in a Fenton reaction system. *Free Radic Res.* 2020:1–9. DOI: 10.1080/10715762.2020.1819995
- [20] Kasahara Y, Ashihara Y. Colorimetry of angiotensin-I converting enzyme activity in serum. *Clin Chem.* 1981;27(11):1922–1925.
- [21] Ueda U, Matsumoto K, Endo K. Evidence of hepatic endogenous hydrogen peroxide in bile of selenium-deficient rat. *Biochem Biophys Res Commun.* 2000;271(3):699–702.
- [22] Ui I, Okajo A, Endo K, et al. Effect of hydrogen peroxide in redox status estimation using nitroxyl spin probe. *Free Radic Biol Med.* 2004;37(12):2012–2017.
- [23] Watanabe T, Tanimoto Y, Sakata T, et al. The magnetic field effects on the electrolysis of hexacyanoferrate(II) oxidation and hexacyanoferrate(III) reduction. *BCSJ.* 1985;58(4):1251–1254.
- [24] Itami Y. Observation of magnetic field effect on decomposition reaction of hydrogen peroxide. *Chemistry & Education.* 1999; 47(5):335–337.
- [25] Mori Y, Sakaguchi Y, Hayashi H. Magnetic field effects on chemical reactions of biradical radical ion pairs in homogeneous fluid solvents. *J Phys Chem A.* 2000;104(21):4896–4905.



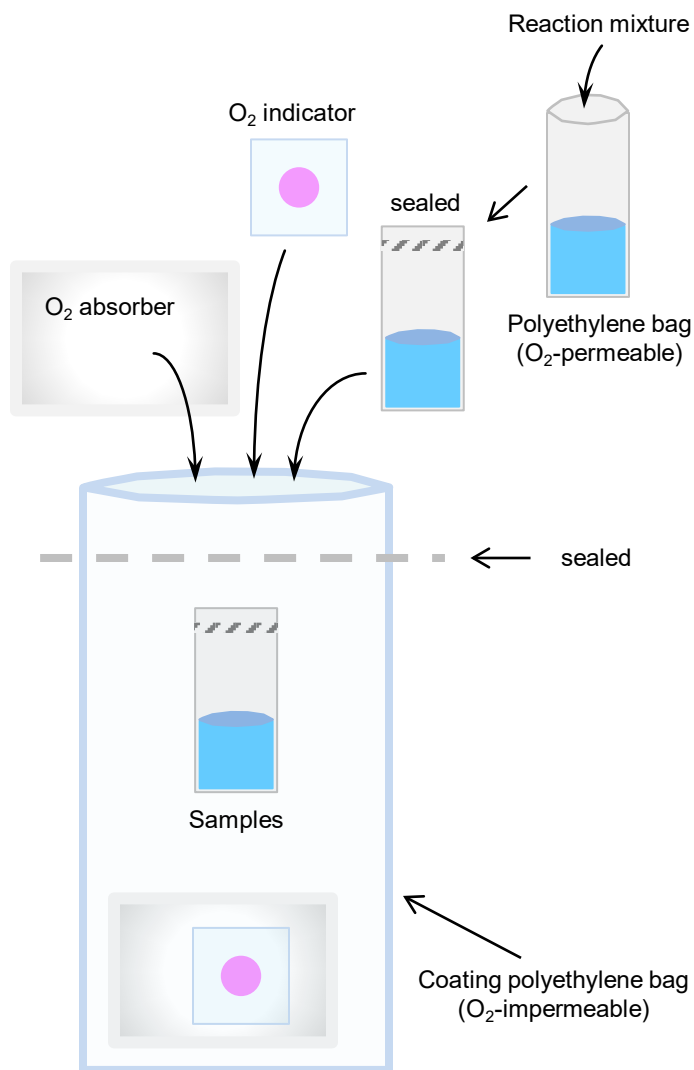
Suppl. Fig. 1. Decay correction of DMPO-OH. (A) The time course of the spin-adduct after irradiation was experimentally measured, and the decay rate of the spin-adduct,  $k_{EXP}$ , and the spin-adduct concentration in the irradiated sample at the end of irradiation,  $C_{0EXP}$ , were estimated. (B) The decay of the spin-adduct during irradiation,  $k_{IRD}$ , was corrected assuming  $k_{IRD} = 3 \times k_{EXP}$  and the net amount of the spin-adduct generated during irradiation,  $C_{ONET}$ , was obtained as  $C_{OSIM}$ , being equal to  $C_{0EXP}$ .



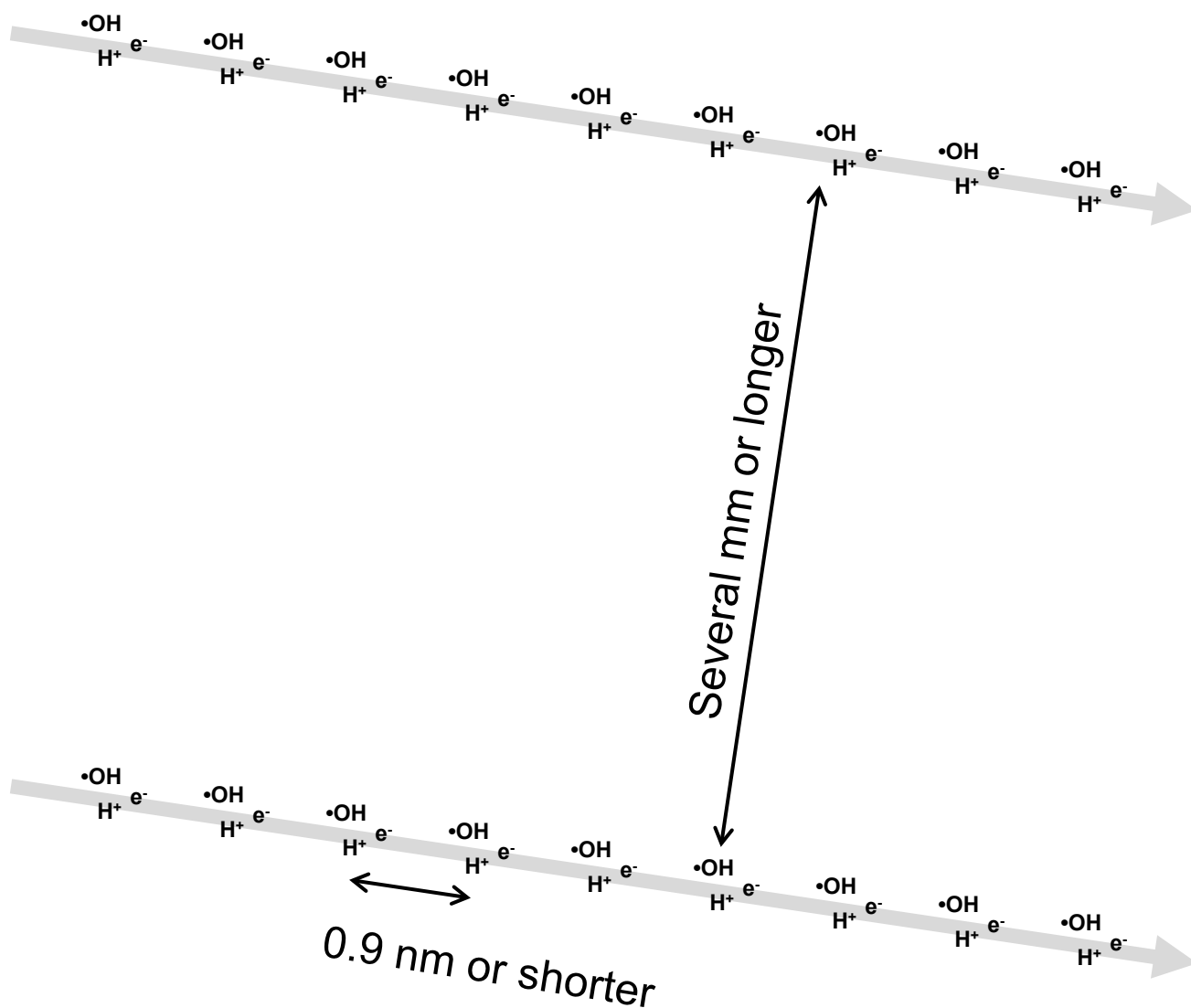
Suppl. Fig. 2. Estimation of first-order decay rates,  $k_{\text{EXP}}$ , of DMPO-OH in water with different concentrations of DMPO. The  $k_{\text{EXP}}$  of DMPO-OH were estimated using a set of X-band EPR signals repeatedly measured after 32-Gy X-ray irradiation of the corresponding DMPO reaction mixture. The EPR measurement was started approximately 2.5–3.0 min and repeated for 10 min with 1-min intervals. (A) Decay of DMPO-OH in 1661 mM (1000  $\mu\text{m}^{-1}$ ) DMPO solution. (B) Decay of DMPO-OH in 0.49 mM (66.7  $\mu\text{m}^{-1}$ ) DMPO solution. Results of independent experiments were plotted in different colors. (C) Relationship of  $k_{\text{EXP}}$  of DMPO-OH with the intermolecular density of DMPO. The  $k_{\text{EXP}}$  of DMPO-OH generated in the reaction mixture irradiated by X-rays were plotted versus the density of the DMPO in the corresponding reaction mixture. For example, marks with dotted circles in (C) are the decay rates experimentally estimated from data sets (A) and (B).



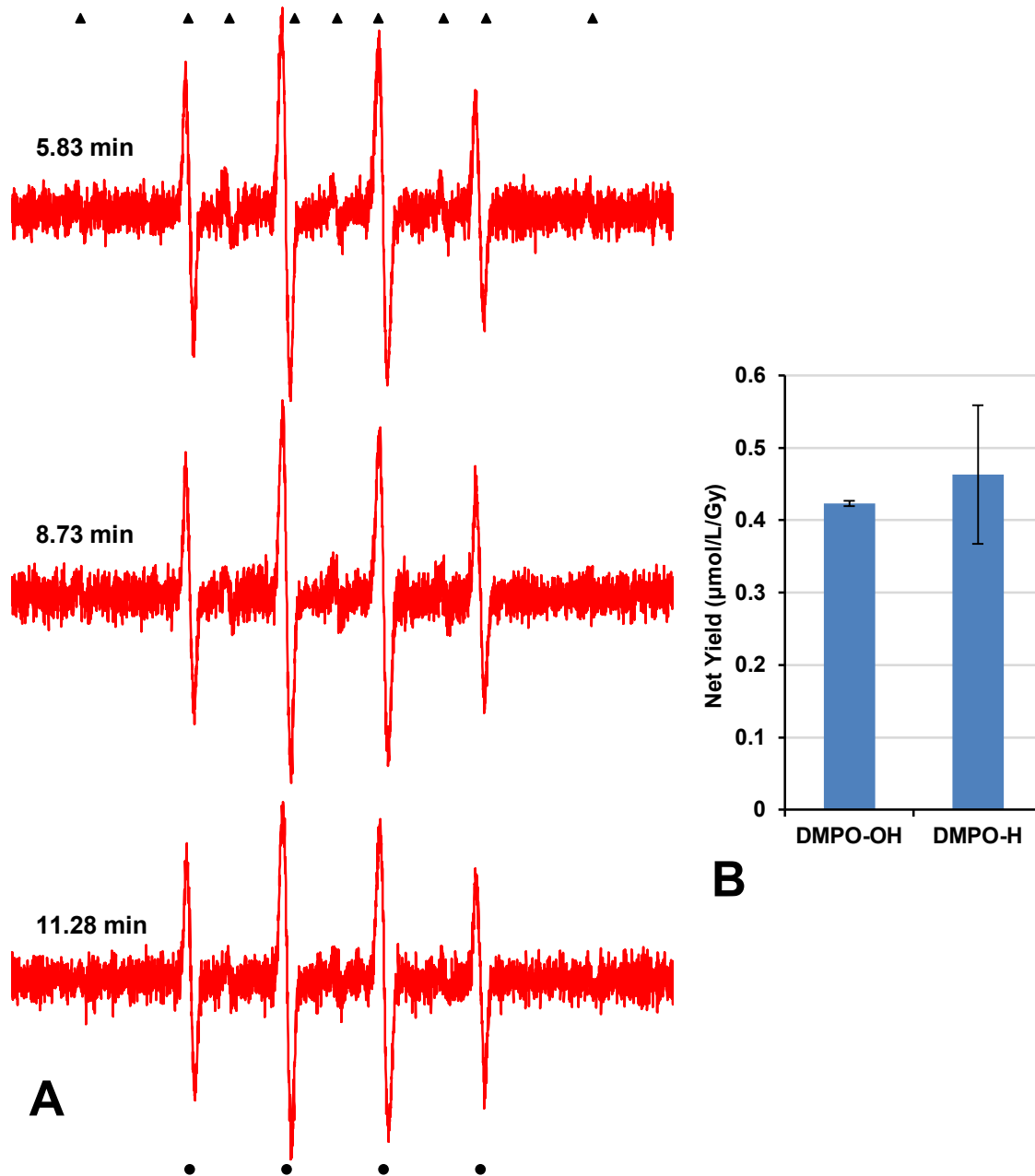
Suppl. Fig. 3. Correction of the decay rate used for the decay correction. The 2.3 M DMPO water solution was irradiated with several doses of X-rays. Estimated net DMPO-OH yields in the sample solutions were plotted against the X-ray dose. The value extrapolated as the DMPO-OH decay to  $t = 0$ ,  $C_{0EXP}$ , i.e., no decay correction (light gray diamond), did not linearly increase with the dose. When the decay during irradiation was corrected assuming  $k_{IRD} = k_{EXP}$  (dark gray triangle), the estimated net yield of DMPO-OH,  $C_{0NET}$ , was not linearly related to the dose. When the decay during irradiation was corrected using  $k_{IRD} = 3.05 \times k_{EXP}$  (black circle), the estimated net yield of DMPO-OH,  $C_{0NET}$ , linearly increased with the X-ray dose.



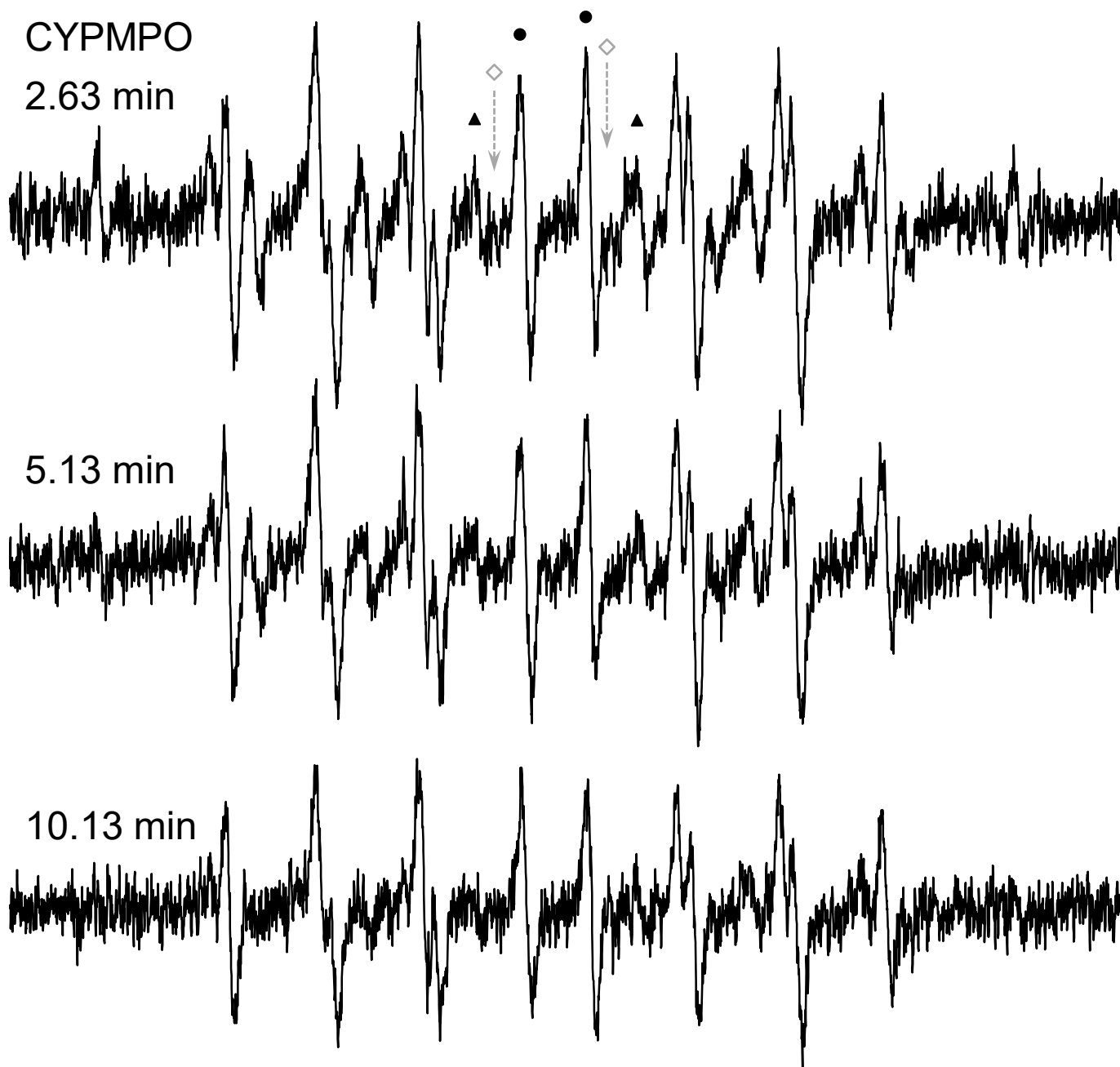
Suppl. Fig. 4. Schematic drawing of the sample preparation for irradiation under hypoxic conditions. An aliquot (300–350  $\mu$ l) of sample solution was sealed in an O<sub>2</sub>-permeable polyethylene bag using a heat sealer. The samples were moved into a glove box, and N<sub>2</sub> gas was pumped into the glove box to establish a 0.5% or lower O<sub>2</sub> atmosphere. The polyethylene bag containing the sample solution was again sealed in an O<sub>2</sub>-impermeable bag with an O<sub>2</sub> absorber and colorimetric O<sub>2</sub> marker.



Suppl. Fig. 5. An image of initial reactive species of water radiolysis, i.e.  $\bullet\text{OH}$ ,  $\text{H}^+$ , and  $e^-$ , on the beam track. When  $2 \times 10^{12}$  particles/sec was irradiated as a beam of 10 cm in diameter, it corresponded to 0.25 particles/ $\text{mm}^2/\text{ns}$ , and the distance between a particle track and the other particle track can be estimated at around 2 mm. The molecular distance of 2 mm corresponds to a concentration of 0.2 aM.



Suppl. Fig. 6. Comparison of net yields of DMPO-OH and DMPO-H caused by carbon-ion beam in 1.7 M DMPO water solution. (A) Time course of the X-band EPR signal observed after carbon-ion beam irradiation. Closed circles indicate the EPR signal of DMPO-OH, which consists of 4 lines with an intensity ratio of 1:2:2:1. Closed triangles indicate the EPR signal of DMPO-H, which consists of 9 lines with an intensity ratio of 1:1:2:1:2:1:2:1:1; some lines overlap. (B) Net yields of DMPO-OH and DMPO-H. The decay rates of DMPO-OH and DMPO-H after irradiation, i.e.,  $k_{\text{EXP}}$ , used for the decay correction were 0.0215 and 0.1968  $\text{min}^{-1}$ , respectively. These decay rates were observed by X-ray experiments. For comparison, the decay rates of DMPO-OH and DMPO-H calculated from results shown in (A) were 0.0198 and 0.1201  $\text{min}^{-1}$ , respectively. The decay rates during irradiation, i.e.  $k_{\text{IRD}}$ , were estimated to be  $3.05 \times k_{\text{EXP}}$  for DMPO-OH and  $1.50 \times k_{\text{EXP}}$  for DMPO-H by X-ray experiments. The variation in the estimated yield of DMPO-H was larger than that of DMPO-OH due to the smaller signal height caused by more hyperfine splitting and faster decay of the EPR signal of DMPO-H.



Suppl. Fig. 7. Time course of the X-band EPR signal observed in a CYPMPO water solution after X-ray irradiation. A 500 mM CYPMPO water solution was irradiated by 32 Gy of X-rays at 3.0 Gy/min. Closed circles indicate the peak of CYPMPO-OH. Gray open diamonds indicate the expected peak positions of CYPMPO-OOH, which were absent on the spectrum. Closed triangles are likely CYPMPO-H due to its relatively fast decay. Only CYPMPO-OH was observed 10 min after X-ray irradiation. The EPR parameters were as follows: microwave frequency was 9.4 GHz, microwave power was 2 mW, center field was 336.7 mT, field sweep width was  $\pm 7.5$  mT, field sweep rate was 7.5 mT/min, time constant was 0.03 s, modulation frequency was 100 kHz, and modulation width was 0.063 mT.